Science Advances
AAAS

advances.sciencemag.org/cgi/content/full/5/12/eaaw5595/DC1

Supplementary Materials for

A minimally invasive lens-free computational microendoscope

Jaewook Shin, Dung N. Tran, Jasper R. Stroud, Sang Chin, Trac D. Tran, Mark A. Foster*

*Corresponding author. Email: mark.foster@jhu.edu

Published 6 December 2019, *Sci. Adv.* **5**, eaaw5595 (2019)
DOI: 10.1126/sciadv.aaw5595

The PDF file includes:

Other Supplementary Material for this manuscript includes the following:

(available at advances.sciencemag.org/cgi/content/full/5/12/eaaw5595/DC1)

Experimental system

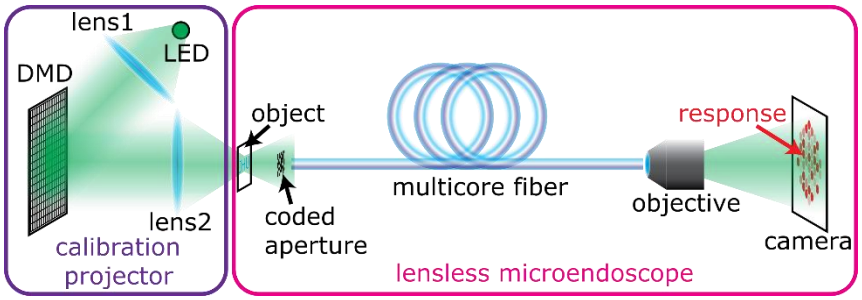

Fig. S1. Detailed schematic of our approach consisting of calibration optics and the imager. The calibration projector includes an incoherent light source (M530L3, MCWHL5 Thorlabs), an aspheric lens (lens 1, ACL5040U-A Thorlabs), a digital micromirror device (DMD, DLP3000, Texas Instruments), and an achromatic lens (lens 2, #49-664 Edmund Optics). Lens 1 is used to collimate the incoherent light onto the DMD while lens 2 is used to image the mirrors of the DMD onto the sample plane with approximately 3.3 de-magnification. Lens 1,2 and the DMD are used to project and scan a point source across the field-of-view of our sample plane. Out of the 684 x 608 DMD pixels, 600 x 300 pixels are used to define the full field-of-view in a single depth plane. A DMD macro pixel is used to generate a square point source of 16.3-µm or 9.78-µm width. The lensless microendoscope includes the coded aperture and a 30-cm-long multicore fiber (FIGH-06-300S, Fujikura) with 270-µm image circle diameter, and 3-µm fiber core diameter and 3.3-µm pitch. A 20X objective lens and a CCD camera (GS3-U3-15S5M-C, Pointgrey) are used to image the proximal end of the multicore fiber, which acquires the system responses of each point source and an object.

Custom scripts were written to automate the data acquisition, which upload a macro pixel on the DMD, acquire a single snapshot from the camera, and repeat for every macro pixel generated across the sample plane. In addition to data acquisition, custom scripts were written to process the coded-aperture response images as we need to acquire the light intensities in each fiber core. A local maxima pursuit algorithm (median filter followed by convolution with a gaussian point spread function) is used to compute the spatial positions of the fiber cores from an image of the multicore fiber, and this core map is piecewise multiplied to every coded-aperture responses to extract the light intensities in each fiber core. This process is repeated for every point source being generated which completes the calibration matrix. The same extraction process is done only once for the single-shot measurement of an object's coded-aperture response, and the image reconstruction algorithm is used to recover the object image.

In the experimental results, the JHU and bat test objects (Fig. 2A,B) are projected images generated using the DMD. Esophagus tissue slide (Fig. 2C), resolution targets (Fig. 3), crosses (Fig. 4) and colored objects (Fig. 5) are real objects placed at the sample plane of the experimental system in fig. S1.

We have summarized the specs of lens-based and lesless microendoscopes below.

Lens-based:
FOV = 0.754 mm^2
Lateral resolution: 24
2D Space Bandwidth Product: 6000
Depth resolution: N/A
Video frame rate: 50 frames per second

Lensless:
FOV = 0.96 mm^2
Lateral resolution: 14 µm
2D Space Bandwidth Product: 19592
Depth resolution: 300 µm
Video frame rate: 50 frames per second

Volumetric reconstruction and axial resolution

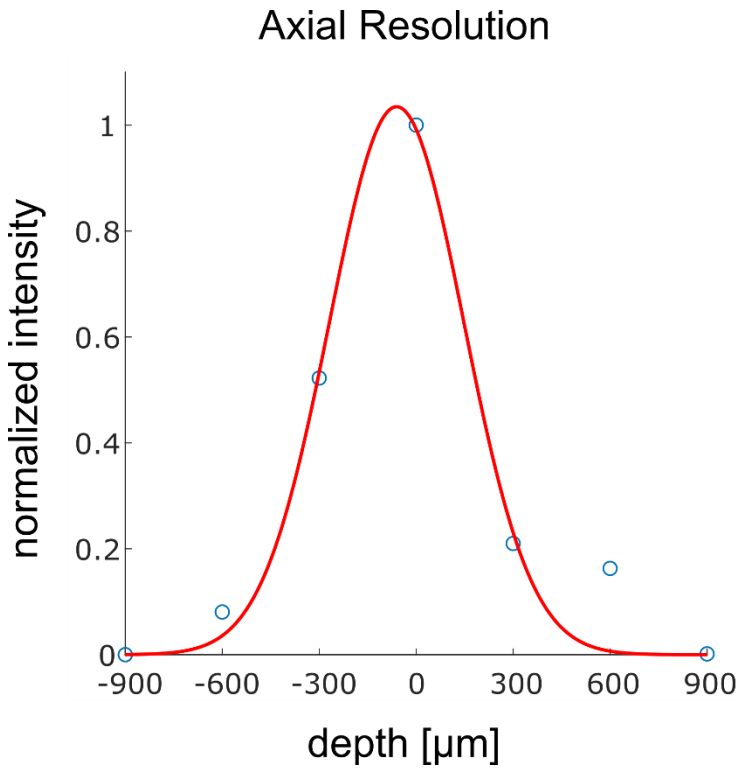

Fig. S2. Determining the axial resolution of the lensless microendoscope. An experimental point source is reconstructed at different depths and the corresponding intensity fall-off is recorded as a function of depth. A fitted Gaussian curve shows that the axial resolution is approximately 300 μm according to the Rayleigh criterion.

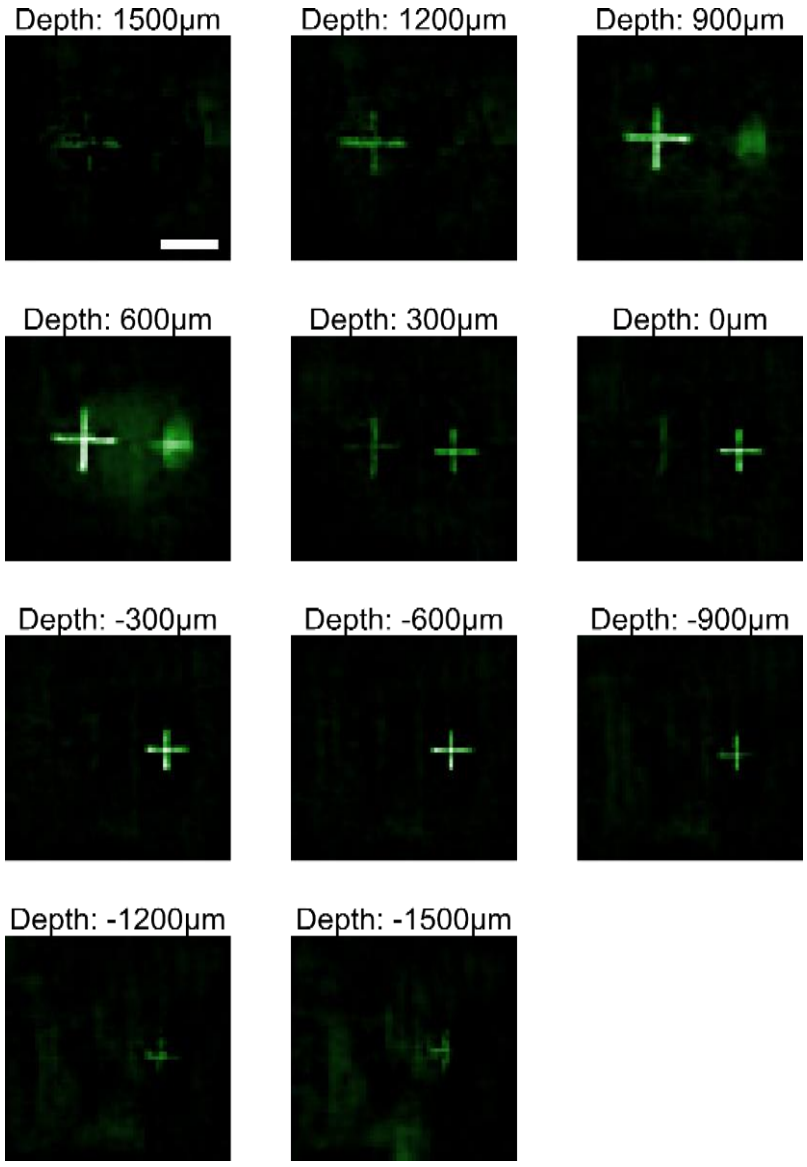

Fig. S3. Volumetric reconstruction of two planar objects separated by 1.5 mm in depth (shown in Figure 4 and movie S2). These 11 figures show the two objects reconstructed at each depth layer. Scalebar = 250 µm.

Spatial resolution comparison

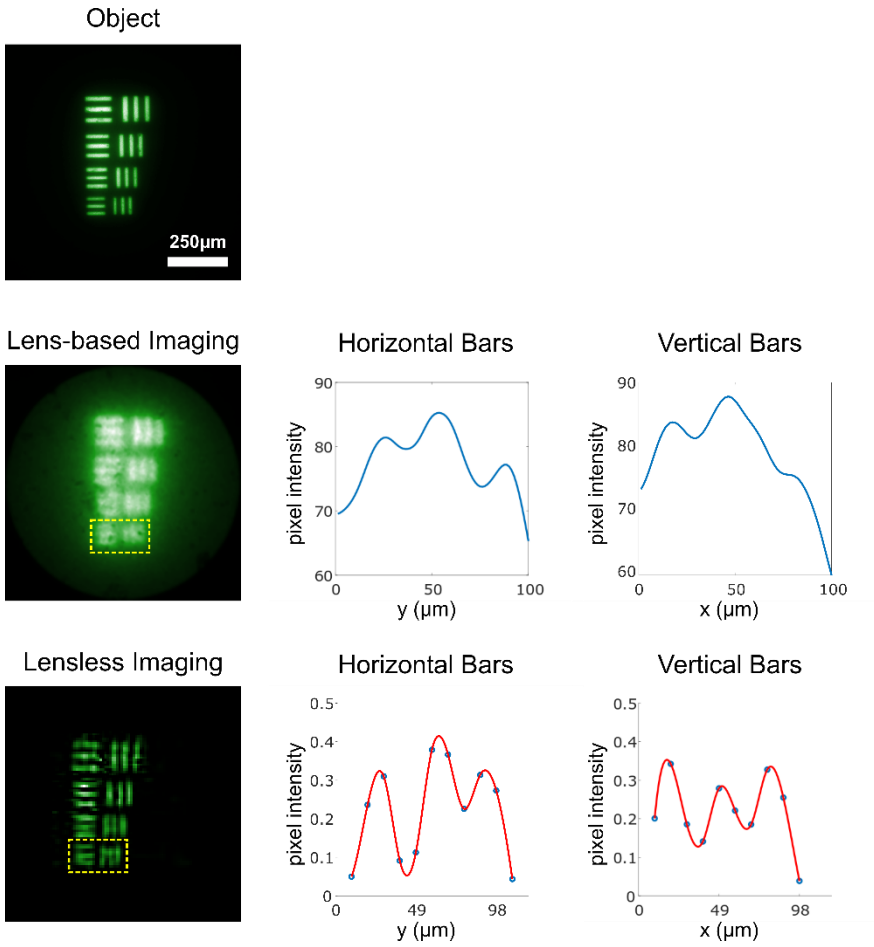

Fig. S4. Comparison of spatial resolution between lens-based and lensless multicore fiber microendoscopes. Above results (Fig. 3 from main body) show resolution targets with linewidths 21 μm, 19 μm, 17 μm, and 14 μm. Lens-based image of the resolution targets is lowpass filtered in order to remove pixelation artifacts due to fiber cores. Regions of interest (yellow dotted lines) show 14 μm linewidths and is used to generate the average horizontal and vertical intensity variations. Line fitting (red curve) in addition to pixel values (blue dots) is used for lensless imaging result, and show that 14 μm linewidths are resolved by the Rayleigh criterion.

Dynamic scene reconstruction

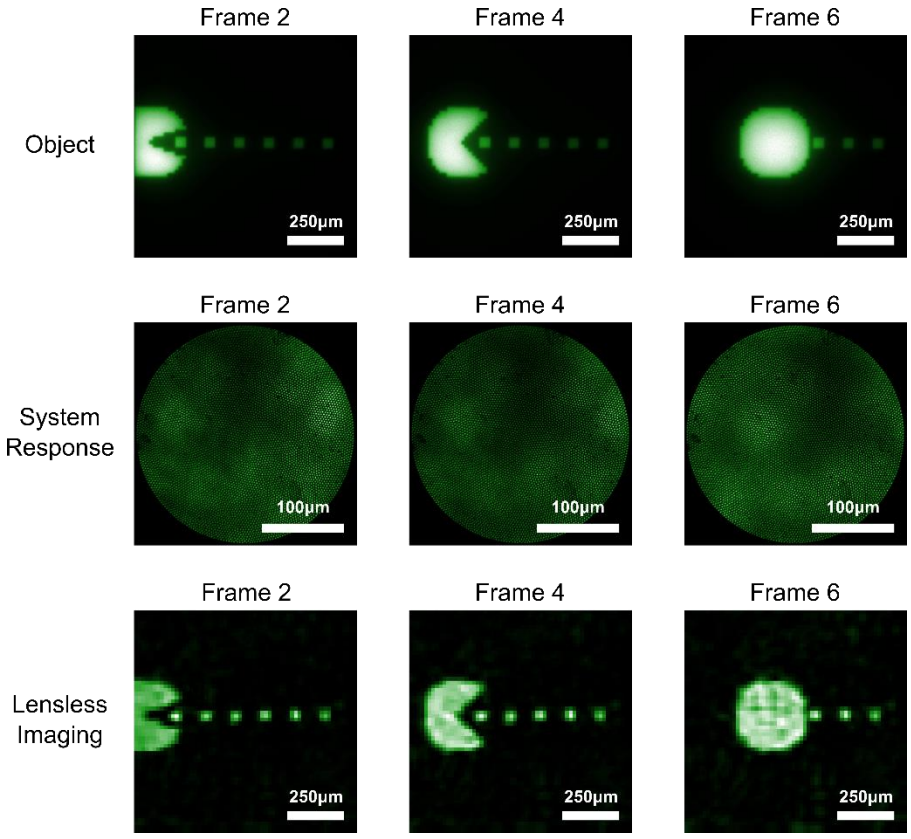

Fig. S5. Demonstration of time-varying scene reconstruction. A moving object is generated using the DMD from fig. S1 and imaged using a lens and a camera. The lensless microendoscope system responses for different frames are acquired at 50 frames per second using the CCD camera and used to reconstruct the scene. A movie of entire 14 frames is included.

Insensitivity to fiber bending

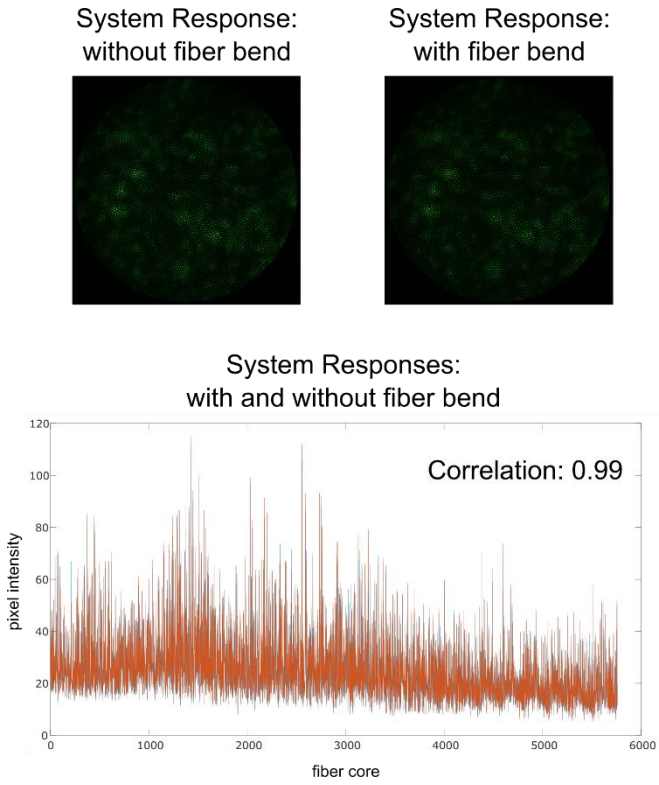

Fig. S6. Demonstration of insensitivity towards bending of the multicore fiber of the lensless microendoscope. The system responses of a point source used in the calibration is shown, both with bending and without bending of the fiber. The 30cm-long multicore fiber is bent approximately by 30^{o} from its normal axis. The light intensities in each fiber core are extracted for both system responses, shown in the bottom figure. The correlation between the two measurements is 0.99, demonstrating the high repeatability and lack of bend sensitivity.